Taylor & Francis
Taylor & Francis Group

Mechanics of Advanced Materials and Structures

ISSN: (Print) (Online) Journal homepage: https://www.tandfonline.com/loi/umcm20

Poisson's ratio of two-dimensional hexagonal materials under finite strains

Xiangzheng Jia, Xiaoang Yuan, Han Shui & Enlai Gao

To cite this article: Xiangzheng Jia, Xiaoang Yuan, Han Shui & Enlai Gao (2023) Poisson's ratio of two-dimensional hexagonal materials under finite strains, Mechanics of Advanced Materials and Structures, 30:4, 751-757, DOI: 10.1080/15376494.2021.2023918

To link to this article: https://doi.org/10.1080/15376494.2021.2023918

Published online: 10 Jan 2022.

MECHANICS OF ADVANCED MATERIALS AND STRUCTURES
2023, VOL. 30, NO. 4, 751–757
https://doi.org/10.1080/15376494.2021.2023918

Taylor & Francis
Taylor & Francis Group

ORIGINAL ARTICLE

Poisson's ratio of two-dimensional hexagonal materials under finite strains

Xiangzheng Jia[#], Xiaoang Yuan[#], Han Shui, and Enlai Gao

Department of Engineering Mechanics, School of Civil Engineering, Wuhan University, Wuhan, Hubei, China

ABSTRACT

Herein, we developed a bead-spring model to predict the Poisson's ratios of two-dimensional hexagonal materials under finite strains. The predicted strain-dependent Poisson's ratios were supported by simulations. The bounds on the Poisson's ratios of two-dimensional hexagonal materials under finite strains (-1/3, $+\infty$) were established. The underlying mechanism for the strain-dependent Poisson's ratios was uncovered as the interplay between bond stretching and angle bending during the stretching. These findings indicate that, even for the simplified material system under finite strains, there is no upper bound on the Poisson's ratios, and that there is plenty of room for strain-engineering the Poisson's ratios.

ARTICLE HISTORY
Received 17 September 2021
Accepted 26 December 2021

KEYWORDS
Finite strains; two-dimensional hexagonal materials; Poisson's ratio; mechanics model; bounds

1. Introduction

The successful exfoliation of graphene from bulk graphite [1] has stimulated considerable interest in two-dimensional (2 D) materials [2–4], and most of the known 2 D materials are hexagonal (named as 2 D hexagonal materials, 2DHMs) [5, 6]. The mechanical behaviors of 2DHMs have been widely explored by theories [7, 8], simulations [9–12] and experiments [13], among which the Poisson's ratio offers a fundamental metric for the elastic behavior.

Poisson's ratio for most materials is positive, while a few auxetic materials exhibit a negative Poisson's ratio (NPR) [14], that is, the materials with the property of transversally expanding rather than shrinking when uniaxially stretched. Materials with NPR are promising for uses in many applications, including enhancing toughness, shear and indentation resistance [15]. Originally, Poisson's ratio is defined for small elastic strains, and thereafter this measure has been generalized for finite strains [16], in which the Poisson's ratio depends on the subjected strain. The Poisson's ratio of many commonly used materials is strain-dependent [17–20], providing additional room for tailoring fantastic properties. Ma et al. [19] demonstrated an unprecedented feature in Pd decorated two-dimensional boron sheet, which expands normal to the direction of stress, regardless of whether it is stretched or compressed. Jiang et al. [20] observed a transition from positive Poisson's ratio to NPR for graphene sheets under finite strains.

NPR of 2DHMs has been extensively studied. Grima et al. [21, 22] found that graphene can be modulated to exhibit NPR by introducing defects that wrinkle the planar sheet. Ho et al. [23] tailored the Poisson's ratio of graphene by patterning periodic rectangular voids of different aspect ratios. Wan et al. [24] showed that the modification of oxidation degree can tune the NPR of graphene oxide. Jiang et al. [25] demonstrated that NPR of hydrogenated graphene can be achieved by modulating the percentage of hydrogenation. Qin et al. [26] performed molecular dynamics simulations and observed NPR in the rippled graphene. Zakharchenko et al. [27] observed NPR of graphene by performing atomistic simulations at extremely high temperature arising from the thermally induced ripples. These explorations indicate that the NPR of 2DHMs can be produced by either introducing defects or wrinkles or ripples. Beyond such processing, Jiang et al. [20] found that an intrinsic NPR emerges in graphene as a result of the interplay between two deformation modes, that is, bond stretching and angle bending. More recently, we developed a mechanics model of 2DHMs for small strains and predicted the bounds on the Poisson's ratios of 2DHMs as (-1/3, +1) [28]. However, this study has focused on the Poisson's ratios of 2DHMs for small strains, leaving the bounds on the Poisson's ratios of 2DHMs under finite strains unexplored.

In this work, we generalized the bead-spring model of 2DHMs into the region of finite strains. Based on this mechanics model, the strain-dependent Poisson's ratios of 2DHMs were predicted. Atomistic simulations supported these predictions. The extended bounds on the Poisson's ratios of 2DHMs under finite strains were established as (-1/3, $+\infty$). Finally, the underlying mechanism for the strain-dependent behavior of Poisson's ratios was revealed as the interplay between the deformation modes of bond stretching and angle bending.

CONTACT Enlai Gao enlaigao@whu.edu.cn Department of Engineering Mechanics, School of Civil Engineering, Wuhan University, Wuhan, Hubei 430072, China.
[#]These authors contribute equally.

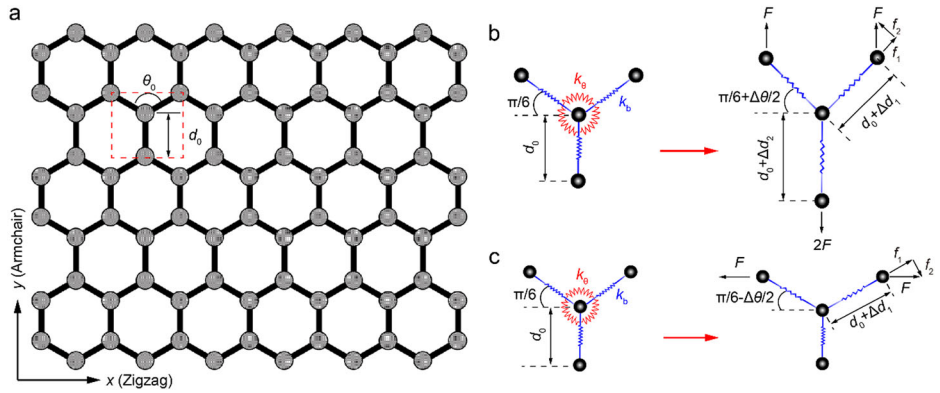

Figure 1. (a) Illustration of 2DHMs. 2DHMs were stretched along the (b) armchair (AC) and (c) zigzag (ZZ) directions, respectively.

2. Methods

Atomistic simulations were performed by large-scale atomic/molecular massively parallel simulator (LAMMPS) [29]. The bond stretching energy is $V_b = k_b(d\text{-}d_0)^2$, and the angle bending energy is $V_a = k_\theta(\theta\text{-}\theta_0)^2$, where k_b, d_0 (d), k_θ, and θ_0 (θ) represent the bond stiffness, equilibrium (deformed) bond length, angle stiffness, and equilibrium (deformed) angle, respectively. Herein, a dimensionless factor $\lambda = k_\theta/(k_b d_0^2)$ is defined to characterize the ratio of angle bending resistance to bond stretching resistance, which measures the contributions of bond stretching and angle bending to overall deformation. As a reference, the values of λ for typical 2 D materials (0.095 for graphene, 0.081 for h-BN, 0.063 for MoS_2, 0.065 for silicene, 0.033 for silica, and 0.092 for black phosphorus [3, 4]) were collected for comparison. Without loss of generality, unitless simulations were conducted, in which the referenced quantities of energy and length were set as ε and σ, and hence d_0 and k_b were used as 1σ and $1\varepsilon/\sigma^2$, respectively. To explore the effect of λ on the Poisson's ratios, k_θ was adopted as $\lambda\varepsilon$. Then, a unit cell of 2DHMs within in-plane periodic boundary conditions was constructed to avoid the size effect. The zigzag (ZZ) and armchair (AC) directions were set to be parallel to the x and y axes, respectively (Figure 1(a)). Uniaxial tensile strain was applied on the 2DHM samples along the x (y) direction with different λ while the freedom in the other direction was fully energy minimized. During the stretching process, the increment of tensile strain was 1% per step, and the strain to failure of bond was set as 16%.

3. Results and discussion

3.1. Mechanics model

Gillis et al. [30] developed a bead-spring model correlating the bond and angle stiffnesses with the elastic properties of hexagonal graphite. Afterward, this model is adopted for uses in the study of Poisson's ratios as well as other mechanical properties of 2DHMs for small strains [3, 28]. Herein, we generalize the bead-spring model into the region of finite strains to explore the strain-dependent behaviors of Poisson's ratio for 2DHMs. The force induced by bond stretching and the torque induced by angle bending can be described as $f = k_b\ (d\text{-}d_0)$ and $T = k_\theta\ (\theta\text{-}\theta_0)$, respectively. When the 2DHM is stretched along the AC direction with a tensile force of $2F$, the unit cell of 2DHM deforms as shown in Figure 1(b). Considering the deformed configuration, F can be decomposed into two components as

$$f_1 = F\sin(\pi/6 + \Delta\theta/2), \tag{1}$$

$$f_2 = F\cos(\pi/6 + \Delta\theta/2), \tag{2}$$

which are parallel and perpendicular to the bond, respectively. Here $\Delta\theta$ is the angle change. The bond length changes induced by f_1 and $2F$ can be described as $\Delta d_1 = f_1/k_b$ and $\Delta d_2 = 2F/k_b$, respectively. Due to the cooperative deformation of angles in the hexagonal ring [30], the angle change can be derived as

$$\Delta\theta = \frac{f_2(d_0 + \Delta d_1)}{3k_\theta}. \tag{3}$$

Combining Eqs. (1)-(3), $\Delta\theta$ can be derived as

$$\Delta\theta = \frac{F\cos(\pi/6 + \Delta\theta/2)[d_0 + F\sin(\pi/6 + \Delta\theta/2)/k_b]}{3k_\theta}. \tag{4}$$

Based on this equation, $\Delta\theta$ can be calculated by numerical methods. In this work, an algorithm combining bisection, secant, and inverse quadratic interpolation methods [31] was adopted to obtain $\Delta\theta$.

Figure 1(b) shows that the original size of the unit cell is $\sqrt{3}d_0 \times 3d_0/2$, while the deformed size can be written as $2(d_0+\Delta d_1)\cos(\pi/6 + \Delta\theta/2)\times[d_0+\Delta d_2+(d_0+\Delta d_1)\sin(\pi/6 + \Delta\theta/2)]$. Thus, the strain can be obtained by

$$\varepsilon_x = \frac{\Delta x}{\sqrt{3}d_0} = \frac{2(d_0 + \Delta d_1)\cos(\pi/6 + \Delta\theta/2) - \sqrt{3}d_0}{\sqrt{3}d_0}, \tag{5}$$

$$\varepsilon_y = \frac{\Delta y}{3d_0/2} = \frac{\Delta d_2 + d_0 + (d_0 + \Delta d_1)\sin(\pi/6 + \Delta\theta/2) - 3d_0/2}{3d_0/2}. \tag{6}$$

The instantaneous Poisson's ratio is given as

$$\nu_y = -\frac{\partial\varepsilon_x}{\partial\varepsilon_y}. \tag{7}$$

Hence, the strain-dependent Poisson's ratios of 2DHM under finite strains can be predicted in the framework of such bead-spring model.

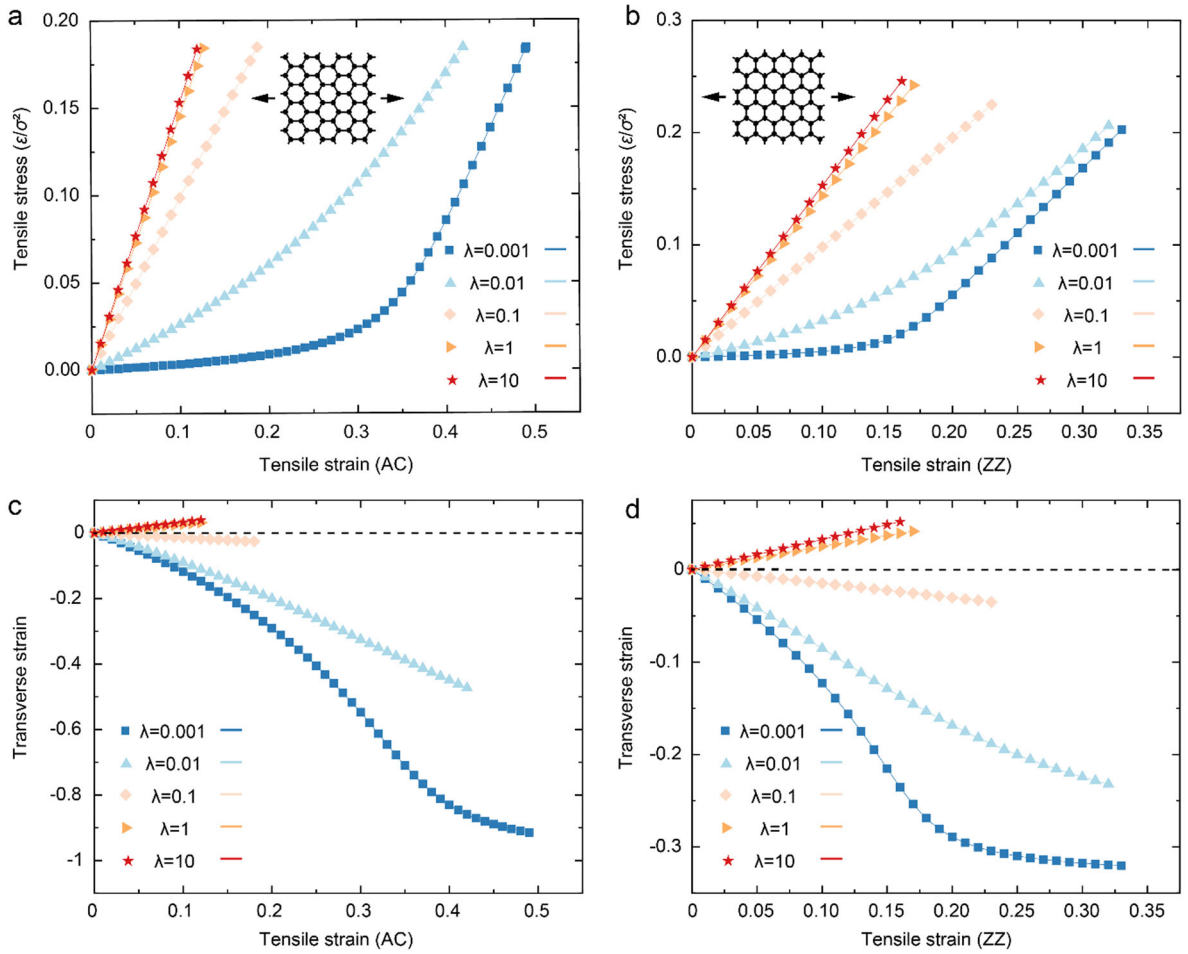

Figure 2. Stress-strain curves of 2DHMs having different λ when stretched along the (a) AC and (b) ZZ directions, respectively. Transverse-tensile strain curves with different λ when stretched along the (c) AC and (d) ZZ directions. Herein, the dots represent the atomistic simulation results and the lines are from the theoretical prediction.

Similarly, as the 2DHM is stretched along the x (ZZ) direction (Figure 1(c)), the corresponding Poisson's ratio of 2DHM can also be derived. Considering the deformed configuration, the force F can be decomposed as

$$f_1 = F\cos(\pi/6 - \Delta\theta/2), \tag{8}$$

$$f_2 = F\sin(\pi/6 - \Delta\theta/2). \tag{9}$$

Combining Eqs. (3), (8) and (9), $\Delta\theta$ can be derived as

$$\Delta\theta = \frac{F\sin(\pi/6-\Delta\theta/2)[d_0 + F\cos(\pi/6-\Delta\theta/2)/k_b]}{3k_\theta}. \tag{10}$$

Figure 1(c) shows that the deformed size of the unit cell is $2(d_0+\Delta d_1)\cos(\pi/6\text{-}\Delta\theta/2)\times[d_0+(d_0+\Delta d_1)\sin(\pi/6\text{-}\Delta\theta/2)]$. Hence, the strain can be obtained by

$$\varepsilon_x = \frac{\Delta x}{\sqrt{3}d_0} = \frac{2(d_0+\Delta d_1)\cos(\pi/6-\Delta\theta/2) - \sqrt{3}d_0}{\sqrt{3}d_0}, \tag{11}$$

$$\varepsilon_y = \frac{\Delta y}{3d_0/2} = \frac{d_0 + (d_0+\Delta d_1)\sin(\pi/6-\Delta\theta/2) - 3d_0/2}{3d_0/2}. \tag{12}$$

The instantaneous Poisson's ratio can be derived as

$$\nu_x = -\frac{\partial\varepsilon_y}{\partial\varepsilon_x}. \tag{13}$$

Notably, previous work [28] on 2DHMs for small strains assumed that the structural symmetry does not change during stretching, and thus changes of $\Delta\theta$ and Δd are negligible. Therefore, the Poisson's ratio is strain-independent. In this work, we consider finite strains that result in the breakdown of structural symmetry, and thus $\Delta\theta$ and Δd cannot be neglected.

3.2. Atomistic simulations

To verify the model prediction, we performed unitless atomistic simulations of uniaxial tensile tests on 2DHMs. k_θ is set as $\lambda\varepsilon$, where λ is adopted as 0.001, 0.01, 0.1, 1 and 10, respectively. For small strains, the Poisson's ratio only depends on the value of λ [28]. However, under finite strains, the Poisson's ratio depends on both λ and the applied strain. The stress-strain responses and transverse-tensile strain responses of 2DHMs when applying uniaxial strain were recorded in Figure 2. The model predictions (lines) were well supported by direct atomistic simulations (dots).

When λ is relatively large, the deformation is dominated by bond stretching, making the structure extremely stiff; when λ is relatively small, the deformation is dominated by angle bending, and thus the structure becomes soft, which results in the increase of ductility. The slopes of the stress-strain curves increase as λ increases (Figure 2(a) and (b)),

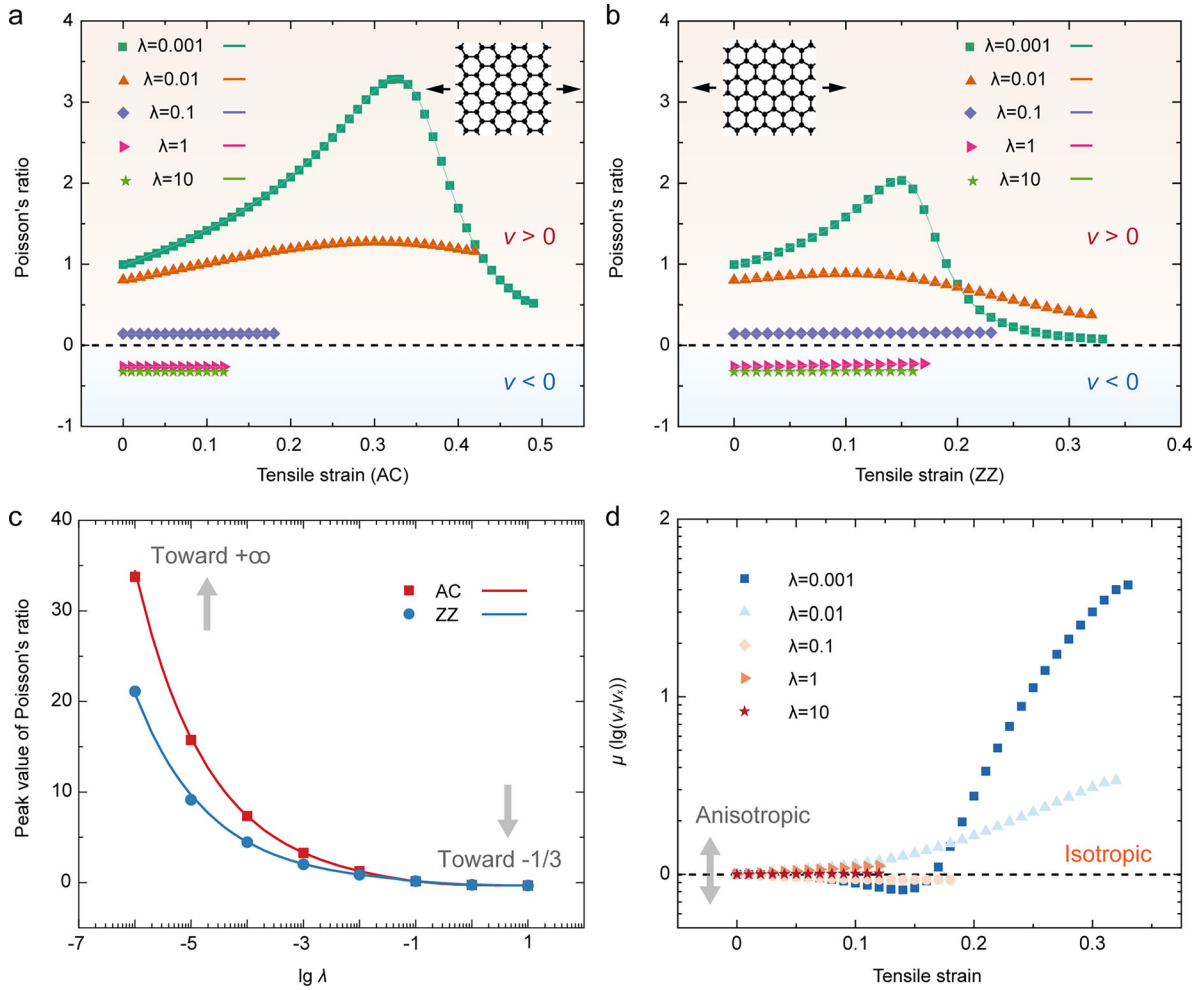

Figure 3. The Poisson's ratio of 2DHMs having different λ as a function of tensile strain when stretched along the (a) AC and (b) ZZ directions. (c) Effect of λ on the peak values of strain-dependent Poisson's ratio. (d) The anisotropy degree μ when subjected to tensile strain.

indicating the increase of Young's modulus. Furthermore, for tensile tests along the ZZ direction (Figure 2(b)), the tensile strength increases while the strain to failure decreases as λ increases. As for tests along the AC direction (Figure 2(a)), the strain to failure decreases while the tensile strength remains constant as λ increases. This behavior of tensile strength can be explained by that Δd_2 is always larger than Δd_1 according to the definitions, and thus the failure is dominated by Δd_2. Additionally, k_b and the maximum permissible Δd_2 remain unchanged in the stretching process, yielding the constant tensile strength.

Furthermore, as shown in Figure 2(a) and (b), when $\lambda = 10$, 1 and 0.1, the stress-strain curves are linear; when $\lambda = 0.01$ and 0.001, the stress-strain curves are nonlinear. Although the styles of bonds and angles are harmonic, the interplay between bond stretching and angle bending results in the linear and nonlinear mechanical behaviors. Notably, when $\lambda = 0.001$, the nonlinear curve transforms to linear curve as strain increases. In this case, the deformation is dominated by angle bending at the beginning of the stretching, and thus the curves are nonlinear. However, as the strain increases until that there is no plenty of room for angle bending, the deformation mode will undergo a transition from angle bending to bond stretching, which results in the linear region. When $\lambda = 0.01$, the deformation is also dominated by angle bending but needs larger strain to achieve the transition of deformation mode, while the structure fails before the linear region emerges. When $\lambda = 0.1$, 1 and 10, the deformation is dominated by the bond stretching, in which the bond can be elongated until failure. Hence, there is no such transition of deformation modes, and the stress-strain curves almost keep linear.

In addition, as shown in Figure 2(c) and (d), when $\lambda = 10$, 1 and 0.1, the transverse-tensile strain curves are linear; when $\lambda = 0.01$ and 0.001, the curves are nonlinear, and the absolute value of the slope firstly increases and then decreases as strain increases. Specifically, the curves become flat as strain increases when $\lambda = 0.001$. The transverse strains are regulated from negative to positive values when λ increases, indicating the NPR behavior. Furthermore, the Poisson's ratio is highly strain-dependent when subjected to uniaxial tensile strain as shown in Figure 3(a) and (b). The different behaviors of 2DHMs along the two directions are mainly caused by the breakdown of structural symmetry. Positive Poisson's ratio decreases to negative value as λ increases. Then, when λ is quite small (for example, λ = 0.001), the Poisson's ratio is highly strain-dependent, which increases from 1 (consistent with the upper bound for small

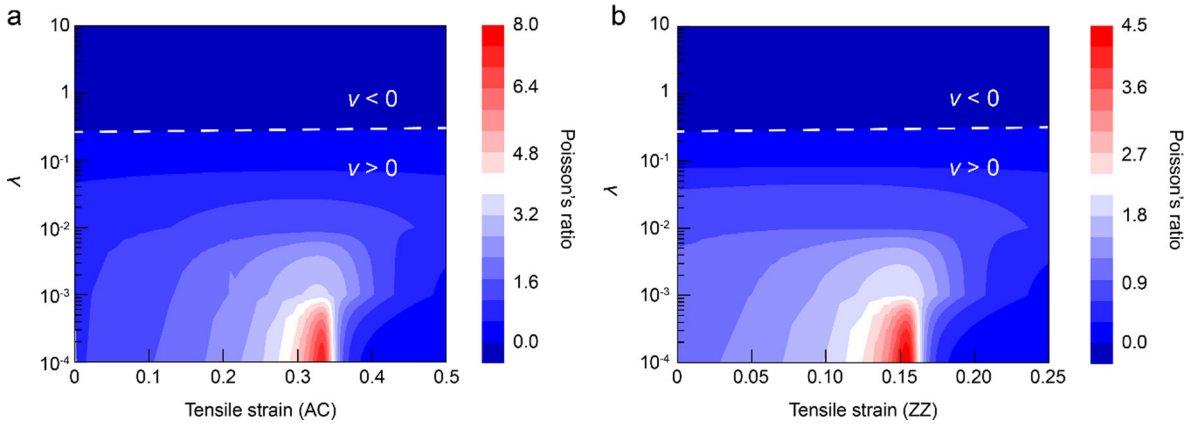

Figure 4. Effect of λ and tensile strain on the Poisson's ratios of 2DHMs when stretched along the (a) AC and (b) ZZ directions.

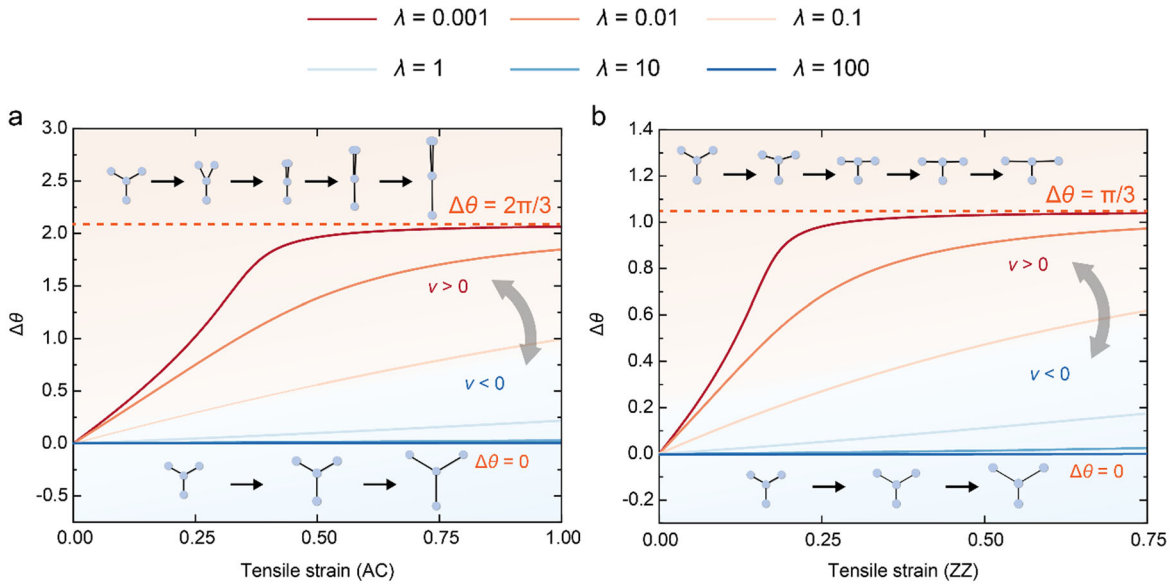

Figure 5. The calculated $\Delta\theta$ of 2DHMs with different λ when the strain is applied along the (a) AC and (b) ZZ directions. The strain-dependent Poisson's ratios of 2DHMs is induced by the interplay between deformation modes of bond stretching and angle bending.

strains [28]) to the peak value and then rapidly decreases toward 0. The underlying mechanism will be discussed later. As λ increases, the Poisson's ratio becomes less dependent on strain, since the structural symmetry is increasingly preserved during the stretching because of the increase of angle bending stiffness. Figure 4 summarizes the Poisson's ratios of 2DHMs as functions of λ and the strain.

Finally, the Poisson's ratio approaches $-1/3$ when $\lambda = 10$, indicating that the lower bound at finite strains is the same as our prediction for small strains [28]. When λ is toward infinity, the angle is too stiff to bend, which means that $\Delta\theta$ equals to approximately 0 in Eqs. (5) and (6) and Eqs. (11) and (12). Also, the transverse-tensile strain curves are linear when λ is toward infinity, indicating the Poisson's ratio as

$$\nu_{y(x)} = -\frac{\partial\varepsilon_{x(y)}}{\partial\varepsilon_{y(x)}} = -\frac{\varepsilon_{x(y)}}{\varepsilon_{y(x)}} = -\frac{1}{3}. \tag{14}$$

However, the maximum value of strain-dependent Poisson's ratio increases as λ decreases, suggesting that there is no upper bound on the Poisson's ratios of 2DHMs under finite strains (Figure 3(c)). Additionally, we defined a dimensionless parameter $\mu = \lg(\nu_y/\nu_x)$ to evaluate the anisotropy of Poisson's ratios. Figure 3(d) shows that μ becomes less strain-dependent as λ increases. These results can be explained by the symmetry of 2DHMs during stretching. The isotropic Poisson's ratio of 2DHMs for small strains is due to the unaltered rotational symmetry of 2DHMs. When λ is relatively large, bond stretching dominates the deformation of 2DHMs and maintains the structural symmetry, and hence μ approaches 0 because of the isotropic feature. Otherwise, the symmetry will be broken by applied uniaxial strains, which results in the remarkable anisotropic Poisson's ratio and highly strain-dependent μ. Furthermore, when the strain-dependent Poisson's ratio reaches the peak value, the corresponding strain along the AC direction is 1/3, larger than that along the ZZ direction $(2\sqrt{3}/3 - 1)$, as shown in Figure 3. When λ is relatively small, there will exist a strain range that ν_y still increases while ν_x rapidly decreases as the tensile strain increases, resulting in the dramatic increase of μ. The smaller λ is, the more drastically the Poisson's ratio changes, and the more rapidly μ increases. However, when $\lambda = 0.001$, μ only slightly decreases before increases, which is attributed to that ν_y increases slower than ν_x in this strain range.

3.3. Mechanism

The mechanism for the strain-dependent Poisson's ratios of 2DHMs under finite strains is explained by the interplay between bond stretching and angle bending. When λ is toward 0, both the axial and transverse deformations of 2DHMs are dominated by angle bending. As the tensile strain increases, the symmetry breaks down and the interplay between bond stretching and angle bending results in a peak Poisson's ratio. This peak Poisson's ratio increases as λ decreases, since it induces more pronounced transverse strain at a certain of axial deformation. However, when angles deform to their limits, the deformation mode will undergo a transition from angle bending to bond stretching, which leads to a relatively small transverse deformation. As a result, the Poisson's ratio drops. Additionally, when $\Delta\theta = 2\pi/3$ and $\pi/3$, the corresponding strains along the AC and ZZ directions are calculated by Eq. (6) and Eq. (11) as $\varepsilon_y = 1/3$ and $\varepsilon_x = 2\sqrt{3}/3 - 1$, respectively. Based on these equations, the applied strains when the strain-dependent Poisson's ratios of 2DHMs having very small λ reach their peak values can be predicted, which are well consistent with direct atomistic simulations (Figure 3(a) and (b)). With the atomic deformation process (the inset of Figure 5(a) and (b)), the subsequent bond stretching causes almost no transverse deformation when the angle change reaches $2\pi/3$ ($\pi/3$) as stretching along the AC (ZZ) direction, suggesting that the Poisson's ratio will decrease to 0. When λ is toward infinity, the deformation is always dominated by bond stretching, and hence the instantaneous Poisson's ratio remains constant (-1/3). In spite of the fact that the assumption of harmonic bonds and angles are not realistic for materials under large deformation, the Poisson's ratios of 2DHMs should lie between the extremes as concluded from this model study.

4. Conclusion

In summary, we developed a mechanics model for predicting the Poisson's ratios of 2DHMs under finite strains. These results show that the lower bound on the Poisson's ratios is $-1/3$, while there is no upper bound on the Poisson's ratios of 2DHMs. Atomistic simulations supported these predictions. Afterwards, the anisotropy of Poisson's ratio of 2DHMs as a function of tensile strain was discussed. Finally, the underlying mechanism of strain-dependent Poisson's ratios of 2DHMs under finite strains was uncovered as the interplay between bond stretching and angle bending. Our work provides new insights into understanding the Poisson's ratios of 2DHMs under finite strains, and guidelines for tuning the Poisson's ratios by modulating the topological interaction and strain engineering.

Acknowledgement

X.J. acknowledges the technical advices from Chunbo Zhang. The numerical calculations in this work have been performed on a supercomputing system in the Supercomputing Center of Wuhan University.

Funding

This work was supported by the National Natural Science Foundation of China (11902225).

Data availability

The data that support the findings of this study are available from the corresponding author upon reasonable request.

References

[1] K. S. Novoselov, et al., Electric field effect in atomically thin carbon films, Science., vol. 306, no. 5696, pp. 666–669, 2004. DOI: 10.1126/science.1102896.

[2] X. Li, L. Gao, W. Zhou, Y. Wang, and Y. Lu, Novel 2D metamaterials with negative Poisson's ratio and negative thermal expansion, Extreme Mech. Lett., vol. 30, pp. 100498, 2019. DOI: 10.1016/j.eml.2019.100498.

[3] E. Gao, S.-Z. Lin, Z. Qin, M. J. Buehler, X.-Q. Feng, and Z. Xu, Mechanical exfoliation of two-dimensional materials, J. Mech. Phys. Solids., vol. 115, pp. 248–262, 2018. DOI: 10.1016/j.jmps.2018.03.014.

[4] E. Gao, and Z. Xu, Thin-shell thickness of two-dimensional materials, J. Appl. Mech., vol. 82, pp. 121012, 2015. DOI: 10.1115/1.4031568.

[5] R. Li, Q. Shao, E. Gao, and Z. Liu, Elastic anisotropy measure for two-dimensional crystals, Extreme Mech. Lett., vol. 34, pp. 100615, 2020. DOI: 10.1016/j.eml.2019.100615.

[6] H. Ding, Z. Zhen, H. Imtiaz, W. Guo, H. Zhu, and B. Liu, Why are most 2D lattices hexagonal? The stability of 2D lattices predicted by a simple mechanics model, Extreme Mech. Lett., vol. 32, pp. 100507, 2019. DOI: 10.1016/j.eml.2019.100507.

[7] S. Y. Davydov, and O. V. Posrednik, On the theory of elastic properties of two-dimensional hexagonal structures, Phys. Solid State., vol. 57, no. 4, pp. 837–843, 2015. DOI: 10.1134/S1063783415040095.

[8] K. H. Michel, and B. Verberck, Theory of elastic and piezoelectric effects in two-dimensional hexagonal boron nitride, Phys. Rev. B., vol. 80, no. 22, pp. 224301, 2009. DOI: 10.1103/PhysRevB.80.224301.

[9] S. Wang, Studies of physical and chemical properties of two-dimensional hexagonal crystals by first-principles calculation, J. Phys. Soc. Jpn., vol. 79, no. 6, pp. 064602, 2010. DOI: 10.1143/JPSJ.79.064602.

[10] R. C. Cooper, C. Lee, C. A. Marianetti, X. Wei, J. Hone, and J. W. Kysar, Nonlinear elastic behavior of two-dimensional molybdenum disulfide, Phys. Rev. B., vol. 87, no. 3, pp. 035423, 2013. DOI: 10.1103/PhysRevB.87.035423.

[11] A. Bezazi, F. Scarpa, and C. Remillat, A novel centresymmetric honeycomb composite structure, Compos. Struct., vol. 71, no. 3–4, pp. 356–364, 2005. DOI: 10.1016/j.compstruct.2005.09.035.

[12] E. Gao, X. Jia, L. Shui, and Z. Liu, Tuning the nonlinear mechanical anisotropy of layered crystals via interlayer twist, J. Appl. Mech., vol. 88, pp. 011007, 2020. DOI: 10.1115/1.4048647.

[13] F. Scarpa, P. Panayiotou, and G. Tomlinson, Numerical and experimental uniaxial loading on in-plane auxetic honeycombs, J. Strain Anal. Eng. Des., vol. 35, no. 5, pp. 383–388, 2000. DOI: 10.1243/0309324001514152.

[14] K. E. Evans, M. A. Nkansah, I. J. Hutchinson, and S. C. Rogers, Molecular network design, Nature., vol. 353, no. 6340, pp. 124–124, 1991. DOI: 10.1038/353124a0.

[15] G. N. Greaves, A. L. Greer, R. S. Lakes, and T. Rouxel, Poisson's ratio and modern materials, Nat. Mater., vol. 10, no. 11, pp. 823–837, 2011. DOI: 10.1038/nmat3134.

[16] C. W. Smith, R. J. Wootton, and K. E. Evans, Interpretation of experimental data for Poisson's ratio of highly nonlinear

materials, Exp. Mech., vol. 39, no. 4, pp. 356–362, 1999. DOI: 10.1007/BF02329817.

[17] K. E. Evans, and A. Alderson, Auxetic materials: Functional materials and structures from lateral thinking!, Adv. Mater., vol. 12, no. 9, pp. 617–628, 2000. DOI: 10.1002/(sici)1521-4095(200005)12:9 < 617::aid-adma617 > 3.0.co;2-3.

[18] G. Qin, and Z. Qin, Negative Poisson's ratio in two-dimensional honeycomb structures, npj Comput. Mater., vol. 6, pp. 51, 2020. DOI: 10.1038/s41524-020-0313-x.

[19] F. Ma, Y. Jiao, W. Wu, Y. Liu, S. A. Yang, and T. Heine, Half-auxeticity and anisotropic transport in Pd decorated two-dimensional boron sheets, Nano Lett., vol. 21, no. 6, pp. 2356–2362, 2021. DOI: 10.1021/acs.nanolett.0c04154.

[20] J.-W. Jiang, T. Chang, X. Guo, and H. S. Park, Intrinsic negative Poisson's ratio for single-layer graphene, Nano Lett., vol. 16, no. 8, pp. 5286–5290, 2016. DOI: 10.1021/acs.nanolett.6b02538.

[21] J. N. Grima, M. C. Grech, J. N. Grima-Cornish, R. Gatt, and D. Attard, Giant auxetic behaviour in engineered graphene, Ann. Phys., vol. 530, no. 6, pp. 1700330, 2018. DOI: 10.1002/andp.201700330.

[22] J. N. Grima, et al., Tailoring graphene to achieve negative Poisson's ratio properties, Adv. Mater., vol. 27, no. 8, pp. 1455–1459, 2015. DOI: 10.1002/adma.201404106.

[23] V. H. Ho, D. T. Ho, S.-Y. Kwon, and S. Y. Kim, Negative Poisson's ratio in periodic porous graphene structures, Phys. Status Solidi B., vol. 253, no. 7, pp. 1303–1309, 2016. DOI: 10.1002/pssb.201600061.

[24] J. Wan, J.-W. Jiang, and H. S. Park, Negative Poisson's ratio in graphene oxide, Nanoscale., vol. 9, no. 11, pp. 4007–4012, 2017. DOI: 10.1039/C6NR08657H.

[25] J.-W. Jiang, T. Chang, and X. Guo, Tunable negative Poisson's ratio in hydrogenated graphene, Nanoscale., vol. 8, no. 35, pp. 15948–15953, 2016. DOI: 10.1039/C6NR04976A.

[26] H. Qin, Y. Sun, J. Z. Liu, M. Li, and Y. Liu, Negative Poisson's ratio in rippled graphene, Nanoscale., vol. 9, no. 12, pp. 4135–4142, 2017. DOI: 10.1039/C6NR07911C.

[27] K. V. Zakharchenko, M. I. Katsnelson, and A. Fasolino, Finite temperature lattice properties of graphene beyond the quasiharmonic approximation, Phys. Rev. Lett., vol. 102, no. 4, pp. 046808, 2009. DOI: 10.1103/PhysRevLett.102.046808.

[28] C. Zhang, N. Wei, E. Gao, and Q. Sun, Poisson's ratio of two-dimensional hexagonal crystals: A mechanics model study, Extreme Mech. Lett., vol. 38, pp. 100748, 2020. DOI: 10.1016/j.eml.2020.100748.

[29] S. Plimpton, Fast parallel algorithms for short-range molecular dynamics, J. Comput. Phys., vol. 117, no. 1, pp. 1–19, 1995. DOI: 10.1006/jcph.1995.1039.

[30] P. P. Gillis, Calculating the elastic constants of graphite, Carbon., vol. 22, no. 4–5, pp. 387–391, 1984. DOI: 10.1016/0008-6223(84)90010-1.

[31] R. P. Brent, Algorithms for Minimization without Derivatives, Prentice-Hall, Englewood Cliffs, NJ, 1973.